

Zhang, G., and Chanson, H. (2018). "Air-water flow properties in stepped chutes with modified step and cavity geometries." *International Journal of Multiphase Flow*, Vol. 99, pp. 423-436 (DOI: 10.1016/j.ijmultiphaseflow.2017.11.009) (ISSN 0301-9322).

Air-Water Flow Properties in Stepped Chutes with Modified Step and Cavity Geometries

Gangfu Zhang, Postdoctoral Research Fellow, School of Civil Engineering,
Univ. of Queensland, Brisbane, QLD 4072, Australia (corresponding author).

E-mail: g.zhang3@uq.edu.au

Hubert Chanson, Professor, School of Civil Engineering,
Univ. of Queensland, Brisbane, QLD 4072, Australia.

E-mail: h.chanson@uq.edu.au

Abstract

Skimming air-water flow properties were investigated in a stepped chute configured with triangular steps, chamfered steps, and partially blocked step cavities. The turbulent interactions between air and water were examined using a synchronised system consisting of a dual-tip phase-detection probe and a pressure transducer mounted side-by-side. In comparison to uniform triangular steps, the chamfered steps were found to cause a reduction in air entrainment and an increase in mean velocity gradient next to the pseudo-bottom. Partial cavity blockages appeared to have little effect on air entrainment, but were linked to an increased presence of large-scale structures in the overflow, which likely resulted from a reduction in mutual sheltering between adjacent step elements. The results indicated that modifications of step and cavity geometries might have significant implications on stepped chute design.

Keywords

Multiphase flow; air entrainment; turbulence; stepped spillway; macro-roughness; chamfer; physical modelling.

Zhang, G., and Chanson, H. (2018). "Air-water flow properties in stepped chutes with modified step and cavity geometries." *International Journal of Multiphase Flow*, Vol. 99, pp. 423-436 (DOI: 10.1016/j.ijmultiphaseflow.2017.11.009) (ISSN 0301-9322).

27 **1. INTRODUCTION**

28 Naturally occurring gas-liquid flows are one of the most challenging hydraulic problems
29 in consequence of the involvement of deformable interfaces and gas compressibility.

30 One classic example is the self-aerated skimming flow in a stepped chute, occurring due
31 to interactions between turbulent boundary layer and free-surface (e.g. Rao and Kobus
32 1971, Wood 1991, Chanson 1997). The air-water mixture downstream of the inception
33 point of aeration is characterised by highly complicated three-dimensional turbulent
34 processes. An example of prototype stepped chute skimming flow is illustrated in
35 Figure 1.

36 The properties and structures of aerated skimming flows were examined by many past
37 studies (e.g. Chanson 1997, Chanson and Toombes 2002a, Felder and Chanson 2014a,
38 2016). To date, most experimental observations are limited to flat steps within prismatic
39 rectangular channels. Several experiments performed for modified bottom geometries
40 have demonstrated modifications of energy dissipation and aeration performance to
41 different extents (e.g. Stephenson (1988) on varying step sizes, Gonzalez and Chanson
42 (2008) on steps with vanes, Felder and Chanson (2014b) on pooled steps, Wuthrich and
43 Chanson (2015) and Zhang and Chanson (2016a) on gabion steps). It is of interest to
44 investigate how modified bottom geometries would affect the air-water flow properties
45 in a stepped chute.

46 The goal of the present study is to investigate the effects of modified step edge and
47 cavity shapes on the two-phase flow properties in aerated skimming flows over stepped
48 chutes. Detailed air-water measurements were performed in stepped chutes configured
49 with triangular steps, chamfered steps, and partially blocked step cavities. The complex
50 two-phase interactions were characterised using a synchronised setup consisting of a
51 dual-tip phase-detection probe mounted abreast of a total pressure transducer. The
52 results revealed some effects of step edge and cavity geometries on air-entrainment and
53 flow structures, which underlined the complexity of stepped chute flows.

Zhang, G., and Chanson, H. (2018). “Air-water flow properties in stepped chutes with modified step and cavity geometries.” *International Journal of Multiphase Flow*, Vol. 99, pp. 423-436 (DOI: 10.1016/j.ijmultiphaseflow.2017.11.009) (ISSN 0301-9322).



54

55 Figure 1 – Hinze dam (Gold Coast, Australia) spillway in operation on 31 Mar 2017 –
56 $q_w \approx 27 \text{ m}^2/\text{s}$, $d_c/h \approx 3.5$, $Re \approx 1.0 \times 10^8$

57 **2. EXPERIMENTAL FACILITIES AND INSTRUMENTATION**

58 2.1 INFLOW CONDITIONS

59 Present investigations were conducted in a large-size stepped spillway model at the
60 University of Queensland (UQ) with very-calm inflow conditions. A smooth and stable
61 discharge was delivered by three pumps driven by adjustable frequency AC motors.
62 Water was fed into a 1.7 m deep, 5 m wide intake basin with a surface area of
63 $2.7 \times 5 \text{ m}^2$, leading to a 2.8 m long side-wall convergent with a contraction ratio of
64 5.08:1, which resulted in a smooth and waveless inflow. The chute inflow was
65 controlled by an upstream broad crested weir. The weir consists of a 1.2 m high, 0.6 m
66 long and 0.985 m wide crest with a vertical upstream wall, an upstream rounded nose
67 (0.058 m radius), and a downstream rounded edge (0.012 m radius). The crest was made
68 of smooth, painted marine ply. The discharge was deduced from integration of velocity
69 profiles measured on the crest (Zhang and Chanson 2016b).

70 2.2 STEPPED SPILLWAY MODELS

71 Detailed two-phase flow studies were conducted in a 45° stepped chute configured with
72 uniform triangular steps and with several modifications to step shape and cavity
73 geometries. The chute details are sketched in Figure 2 and summarised in Table 1.
74 Initial experiments were performed with twelve identical triangular steps ($0.1 \times 0.1 \times 1$

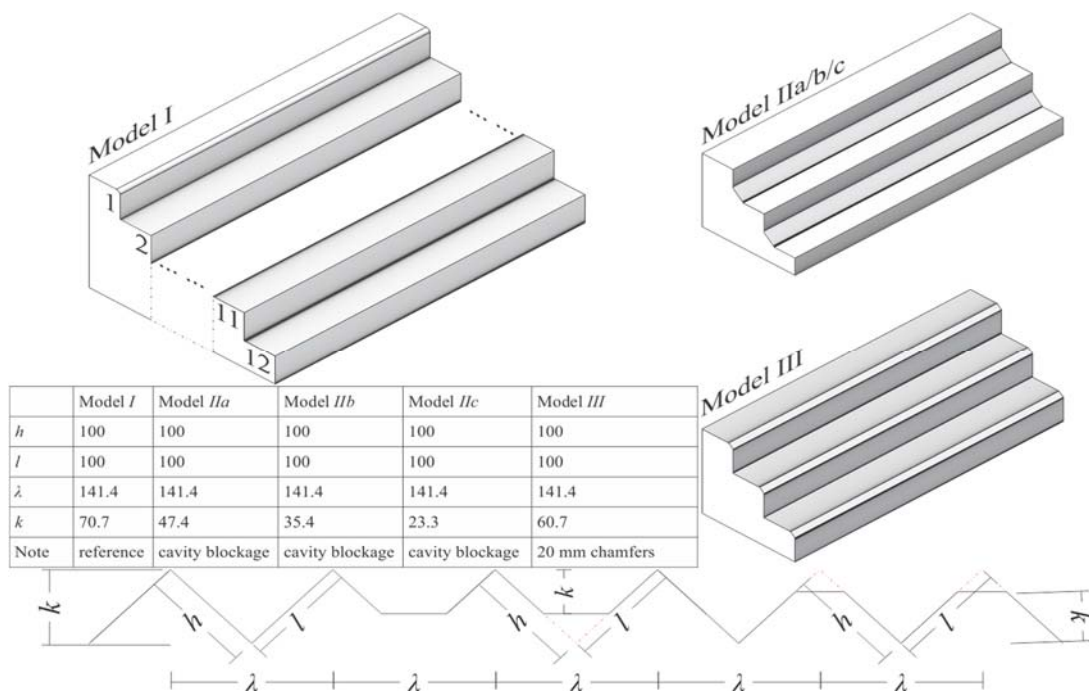
Zhang, G., and Chanson, H. (2018). “Air-water flow properties in stepped chutes with modified step and cavity geometries.” *International Journal of Multiphase Flow*, Vol. 99, pp. 423-436 (DOI: 10.1016/j.ijmultiphaseflow.2017.11.009) (ISSN 0301-9322).

75 m, Fig. 2, top-left). Additional studies were undertaken for three cases of modified
 76 cavity geometries, where the step cavities were blocked to 33%, 50%, and 66% of the
 77 step height, corresponding to roughness densities $\lambda/k = 3, 4, 6$ (Fig. 2, top-right), with λ
 78 the streamwise separation between adjacent step edges and k the step roughness height.
 79 Finally, the effects of step edge modification were examined by replacing step edges 2 –
 80 12 with 20 mm chamfers (Fig. 2, bottom-right).

81 Table 1 – Experimental channel details

Model	h (m)	l (m)	λ (m)	k (m)	λ/k	θ (°)	Modification
<i>I</i>	0.1	0.1	0.14	0.071	2	45	Smooth triangular cavities (i.e. no modification)
<i>IIa</i>	0.1	0.1	0.14	0.047	3	45	Partially filled cavities
<i>IIb</i>				0.035	4		
<i>IIc</i>				0.024	6		
<i>III</i>	0.1	0.1	0.14	0.061	2.33	45	Chamfered step edges

82 Notes: h – vertical step height; l – step length; λ – roughness wavelength; k – roughness height; θ – chute
 83 slope



84
 85 Figure 2 – Definition sketch of experimental configurations (units: mm).

Zhang, G., and Chanson, H. (2018). “Air-water flow properties in stepped chutes with modified step and cavity geometries.” *International Journal of Multiphase Flow*, Vol. 99, pp. 423-436 (DOI: 10.1016/j.ijmultiphaseflow.2017.11.009) (ISSN 0301-9322).

86 2.3 INSTRUMENTATION AND EXPERIMENTAL FLOW CONDITIONS

87 The present experiments were performed with water discharges ranging between $Q =$
88 0.083 and 0.216 m³/s, with a focus on the skimming flow regime. The corresponding
89 Reynolds number range was $3.4 - 8.8 \times 10^5$. For all models, the air-water flow
90 properties were recorded with dual-tip phase-detection probes with an inner tip diameter
91 of 0.25 mm and longitudinal tip separations Δx between 4.3 and 8 mm. For models *I*
92 and *Ila*, additional data were obtained by simultaneously sampling a dual-tip phase-
93 detection probe mounted abreast of a total pressure transducer (inner diameter: 1 mm;
94 outer diameter: 4 mm) to further characterise the turbulent air-water interactions. The
95 pressure transducer was calibrated to measure relative pressures between 0 and 0.15
96 bars at a precision of 0.5% full scale (FS). The details of the experimental flow
97 conditions and sampling parameters are summarised in Table 2.

98 Table 2 – Experimental flow conditions for detailed clear-water and air-water flow
99 measurements

Model	θ (°)	h (m)	W (m)	λ/k	Location	Q (m ³ /s)	d/h	Re	Instrumentation* ¹
<i>I</i>	45	0.1	1.0	2	Step	0.057	0.70 –	2.3 –	DPP: 20 kHz / 45 s
					edges 5 –	–	1.70	8.8×10^5	
					12	0.216			
					Step	0.083	0.90 –	3.4 –	DPP / TPT: 5 kHz / 180 s
edges 5 –	–	1.70	8.8×10^5						
12	0.216								
<i>Ila</i>	45	0.1	1.0	3	Step	0.083	0.90 –	3.4 –	DPP: 20 kHz / 45 s
					edges 4 –	–	1.70	8.8×10^5	
					12	0.216			
					Step	0.083	0.94 –	3.6 –	DPP / TPT: 5 kHz / 180 s
edges 3 –	–	1.75	9.1×10^5						
12	0.182								
<i>Ilb</i>	45	0.1	1.0	4	Step	0.083	0.90 –	3.4 –	DPP: 20 kHz / 45 s
					edges 4 –	–	1.70	8.8×10^5	
12	0.216								
<i>Ilc</i>	45	0.1	1.0	6	Step	0.083	0.90 –	3.4 –	DPP: 20 kHz / 45 s
					edges 4 –	–	1.70	8.8×10^5	
12	0.216								
<i>III</i>	45	0.1	1.0	2.33	Step	0.083	0.90 –	3.4 –	DPP: 20 kHz / 45 s
					edges 5 –	–	1.50	7.3×10^5	
					12	0.182			DPP / TPT: 5 kHz / 180 s

100 Notes: *1 – DPP: Dual-tip Phase-detection probe; TPT: Total pressure transducer.

Zhang, G., and Chanson, H. (2018). “Air-water flow properties in stepped chutes with modified step and cavity geometries.” *International Journal of Multiphase Flow*, Vol. 99, pp. 423-436 (DOI: 10.1016/j.ijmultiphaseflow.2017.11.009) (ISSN 0301-9322).

101 **3. AIR-WATER FLOW PROPERTIES**

102 3.1 BASIC AIR-WATER FLOW PROPERTIES

103 Basic air-water properties at step edges were investigated for all step roughness types
 104 for skimming flow discharges ranging between $d_c/h = 0.9 - 1.5$, where d_c is the critical
 105 flow depth, and h the step height. For all models, the aerated flow was divided into an
 106 initial rapidly varied flow (RVF) region immediately downstream of the inception point
 107 of free-surface aeration, followed by a gradually varied flow region (GVF). In the RVF
 108 region, advective transport is negligible compared with turbulent diffusion, and the void
 109 fraction profiles may be modelled with a theoretical solution (Zhang and Chanson
 110 2017):

$$111 \quad C = \frac{1}{2} \operatorname{erfc} \left(\frac{Y_{50} - y}{2\sqrt{D_a t}} \right) \quad (1)$$

112 where C is the void fraction, y is the normal distance measured from the pseudo-bottom,
 113 Y_{50} the elevation where $C = 0.5$, t is the diffusion time, and D_a is an average diffusivity:

$$114 \quad D_a = \frac{1}{t} \int_0^t D_t dt \quad (2)$$

115 where D_t is a turbulent diffusivity. The similarity between Equation (1) and a Gaussian
 116 cumulative distribution function (CDF) with a mean of Y_{50} and standard deviation of
 117 $\sqrt{2D_a t}$ emphasises the random nature of the initial diffusion process.

118 Further downstream, the aerated flow approaches an approximate equilibrium, where
 119 the effects of bubble buoyancy and droplet weight become relevant. Assuming a
 120 homogeneous air-water mixture between $C = 0$ and 0.9 (Wood 1985, Chanson 1993), a
 121 solution is obtained by balancing the turbulent diffusion and advection terms in the
 122 advection-diffusion equation (Chanson and Toombes 2002a):

$$123 \quad C = 1 - \tanh^2 \left[K - \frac{y'}{2D_0} + \frac{\left(y' - \frac{1}{3} \right)^3}{3D_0} \right] \quad (3)$$

Zhang, G., and Chanson, H. (2018). "Air-water flow properties in stepped chutes with modified step and cavity geometries." *International Journal of Multiphase Flow*, Vol. 99, pp. 423-436 (DOI: 10.1016/j.ijmultiphaseflow.2017.11.009) (ISSN 0301-9322).

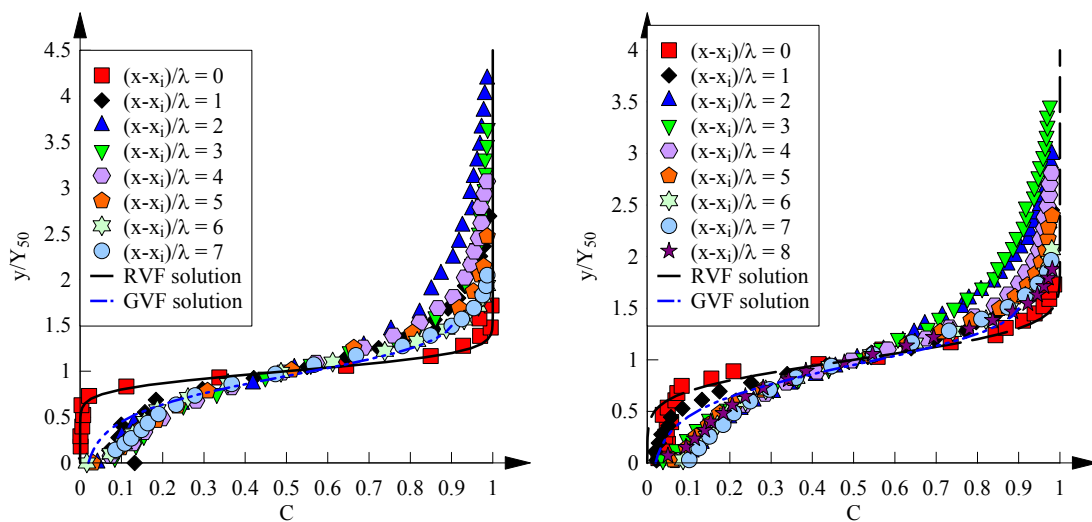
124 where Y_{90} is the elevation where $C = 0.9$, K is an integration constant and D_0 is a
 125 function of C_{mean} :

$$126 \quad C_{\text{mean}} = \frac{1}{Y_{90}} \int_0^{Y_{90}} C dy \quad (4)$$

$$127 \quad K = \tanh^{-1}(\sqrt{0.1}) + \frac{1}{2D_0} - \frac{8}{81D_0} \quad (5)$$

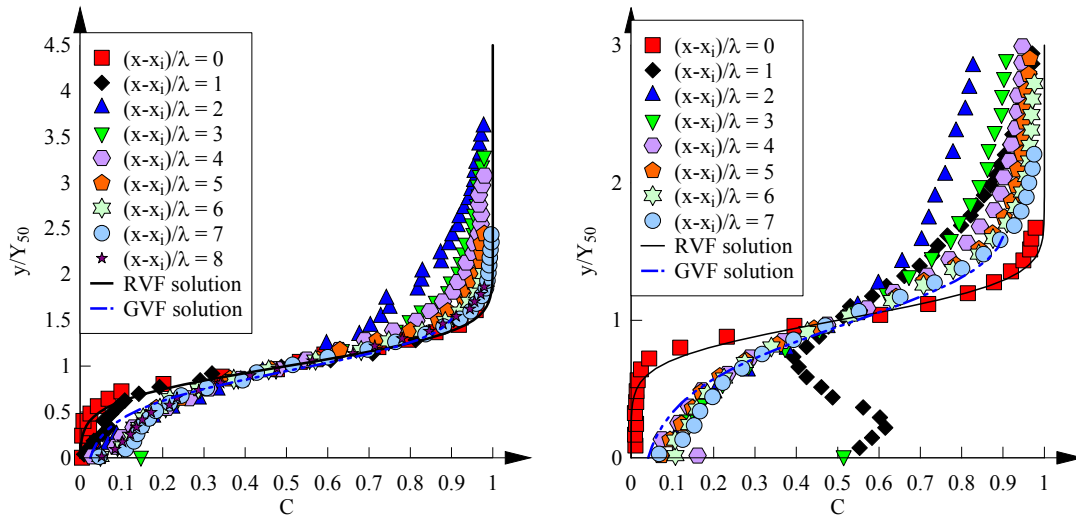
$$128 \quad D_0 = -\frac{1}{3.614} \ln\left(1.0434 - \frac{C_{\text{mean}}}{0.7622}\right) \quad (6)$$

129 Figure 3 presents the dimensionless step edge void fraction distributions in all setups for
 130 a skimming flow $d_c/h = 0.9$, where x is the streamwise distance measured from the first
 131 step edge, x_i is the inception point location, and λ is the separation between adjacent step
 132 edges ($= 0.141$ m). The theoretical solutions (Eqs. 1 and 3) were also plotted for ease of
 133 reference. A good agreement between experimental data and theoretical models was
 134 observed for all models with sharp edges (i.e. models *I*, *IIa*, *IIb*, *IIc*). In model *III* (Figs.
 135 3e-f), the no-flux boundary condition at the chamfer surface appeared to be associated
 136 with the build-up of some air-concentration boundary layer. The observation was
 137 consistent with those in chute and tunnel spillways, and might contribute to a reduction
 138 in skin friction (Chanson 2004). The results suggested that the air concentration profiles
 139 were more influenced by step edge profiles than by cavity shapes.



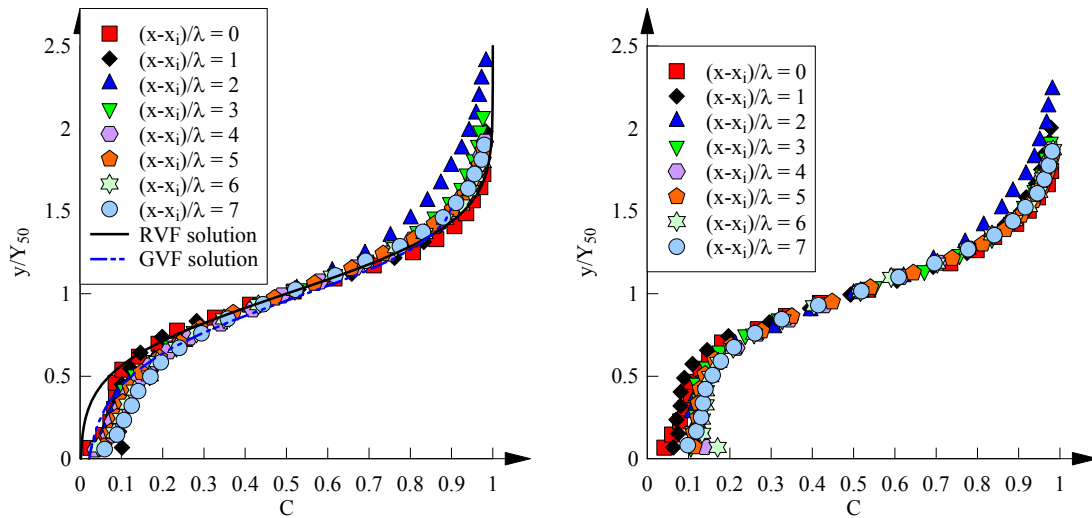
(a) model *I*

(b) model *IIa*



(c) model *IIb*

(d) model *IIc*



(e) model *III*, upstream edge

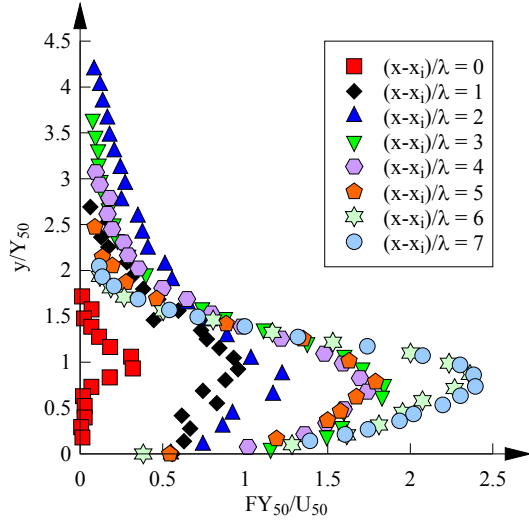
(f) model *III*, downstream edge

140 Figure 3 – Step edge void fraction distributions in chutes with various step roughness
 141 types. Flow conditions: $d_c/h = 0.9$, $Re = 3.4 \times 10^5$, $\theta = 45^\circ$.

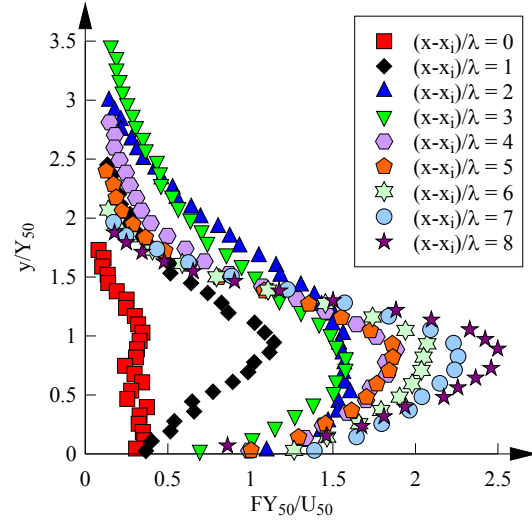
142 The bubble count rate F is defined as half the number of air-water interfaces detected by
 143 the probe sensor per second. For a given interfacial velocity, it is directly proportional
 144 to the specific interfacial area (Chanson 2001b). Figure 4 presents typical skimming
 145 flow bubble count rate distributions in all setups for a dimensionless discharge $d_c/h =$
 146 0.9 . All data exhibited a characteristic bell shape with a marked maximum at $y/Y_{50} \approx 1$
 147 ($C \approx 0.5$), consistent with previous studies (e.g. Chanson and Toombes 2002a, Toombes
 148 and Chanson 2008). Furthermore, a continuous increase in maximum bubble count rate
 149 with increasing distance downstream of the inception was observed in all setups,

Zhang, G., and Chanson, H. (2018). "Air-water flow properties in stepped chutes with modified step and cavity geometries." *International Journal of Multiphase Flow*, Vol. 99, pp. 423-436 (DOI: 10.1016/j.ijmultiphaseflow.2017.11.009) (ISSN 0301-9322).

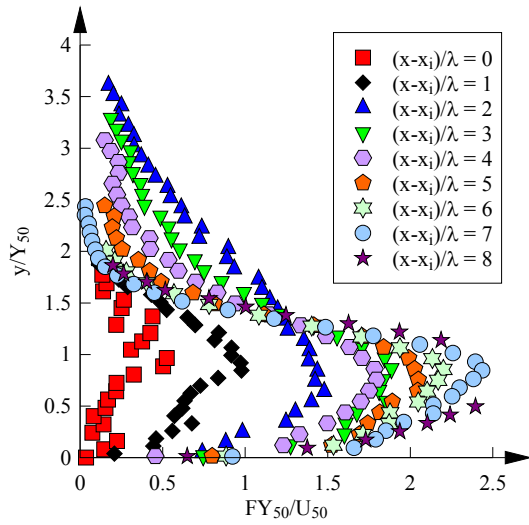
150 implying that uniform equilibrium conditions were not achieved. Overall, the step edge
 151 and cavity modifications appear to have no significant influence on the bubble count
 152 rate profiles.



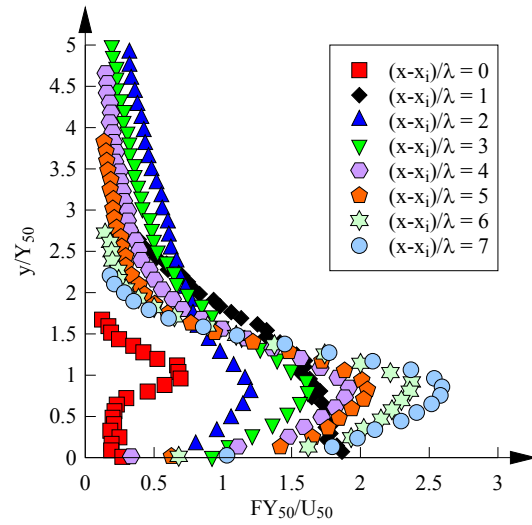
(a) model I



(b) model IIa

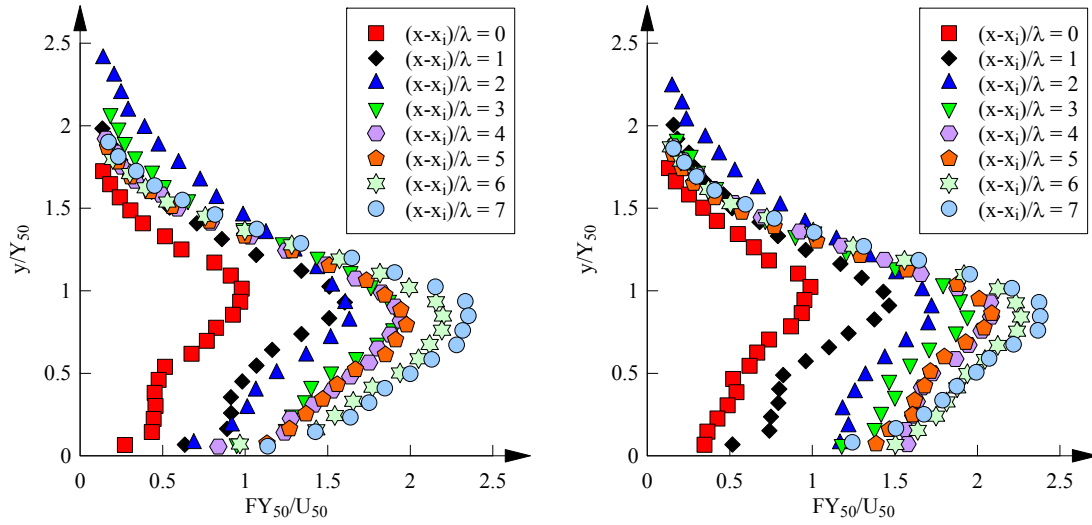


(c) model IIb



(d) model IIc

Zhang, G., and Chanson, H. (2018). “Air-water flow properties in stepped chutes with modified step and cavity geometries.” *International Journal of Multiphase Flow*, Vol. 99, pp. 423-436 (DOI: 10.1016/j.ijmultiphaseflow.2017.11.009) (ISSN 0301-9322).



(e) model III, upstream edge

(f) model III, downstream edge

153 Figure 4 – Step edge bubble count rate distributions in chutes with various step
 154 roughness types. Flow conditions: $d_c/h = 0.9$, $Re = 3.4 \times 10^5$, $\theta = 45^\circ$.

155 The interfacial velocity may be derived from the cross-correlation function between two
 156 probe signals (Crowe et al. 1998, Chanson 2002, Chanson and Carosi 2007):

$$157 \quad U_{aw} = \frac{\Delta x}{T_{aw}} \quad (7)$$

158 where U_{aw} is the interfacial velocity, Δx is the streamwise tip separation and T_{aw} is the
 159 time lag at which the cross-correlation function peaks. Figure 5 shows the step edge
 160 interfacial velocity profiles for all models, where U_{50} is the interfacial velocity
 161 corresponding to $C = 0.5$. All data followed a two-tier distribution:

$$162 \quad \frac{U_{aw}}{U_{50}} = \left(\frac{y}{Y_{50}} \right)^{\frac{1}{N_{50}}} \quad \text{for } 0 \leq y/Y_{50} < 1 \quad (8)$$

163 and

$$164 \quad \frac{U_{aw}}{U_{50}} = 1 \quad \text{for } y/Y_{50} \geq 1 \quad (9)$$

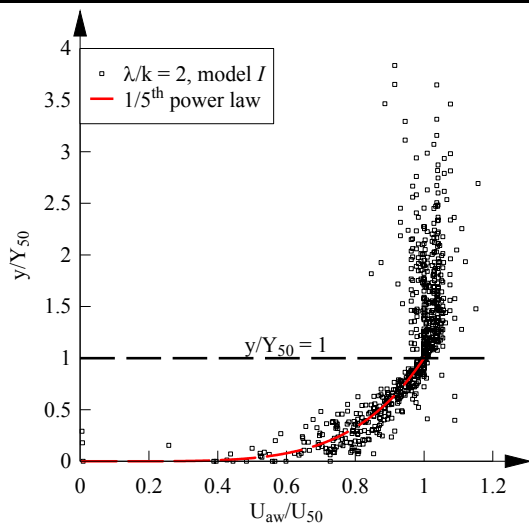
165 Equations (8) and (9) imply a physical demarcation in terms of the flow composition at
 166 about $y/Y_{50} = 1$. A constant interfacial velocity profile for $y/Y_{50} > 1$ implied lesser shear
 167 stress in this region, despite the visually complex nature of the mixture. It also appeared

Zhang, G., and Chanson, H. (2018). “Air-water flow properties in stepped chutes with modified step and cavity geometries.” *International Journal of Multiphase Flow*, Vol. 99, pp. 423-436 (DOI: 10.1016/j.ijmultiphaseflow.2017.11.009) (ISSN 0301-9322).

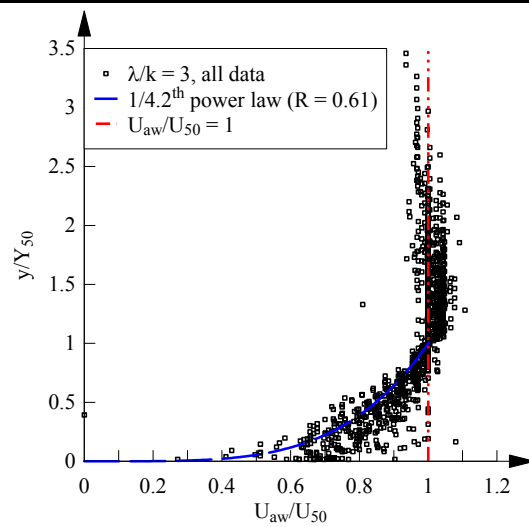
168 that the dynamics of air had little observable effect on the mean momentum of the water
 169 droplets in the spray zone ($C > 0.9$). Table 3 summarises the best fit of power law
 170 exponent N_{50} , and corresponding correlation coefficients R . For all present data, N_{50}
 171 ranged between 3.1 – 7.6. Compared to the non-modified chute (*I*), those with modified
 172 step cavities (*Ila,b,c*) recorded smaller N_{50} values, possibly linked to a downward shift
 173 in the mean velocity profile. In the chamfered chute (*III*), the N_{50} values were larger at
 174 the upstream edge than at the downstream chamfer edge, which could be linked to some
 175 flow separation at the upstream edge. Furthermore, the cavity and step edge
 176 modifications appeared to have respectively resulted in a decrease and an increase in the
 177 correlation coefficient R . The observation was likely reflective of geometry-induced
 178 changes in vortex shedding behaviours, which in turn lead to some streamwise
 179 variations in the overflow.

180 Table 3 – Interfacial velocity power law exponents in all present configurations
 181 (average over all data)

<i>Model</i>	N_{50}	R	<i>Remark</i>
<i>I</i>	5.0	0.75	$\lambda/k = 2$, triangular steps
<i>Ila</i>	4.2	0.61	$\lambda/k = 3$, partially blocked cavities
<i>Ilb</i>	3.1	0.31	$\lambda/k = 4$, partially blocked cavities
<i>Ilc</i>	5.0	0.70	$\lambda/k = 6$, partially blocked cavities
<i>III (upstream edge)</i>	7.6	0.89	$\lambda/k = 2.33$, chamfered steps
<i>III (downstream edge)</i>	5.1	0.95	$\lambda/k = 2.33$, chamfered steps

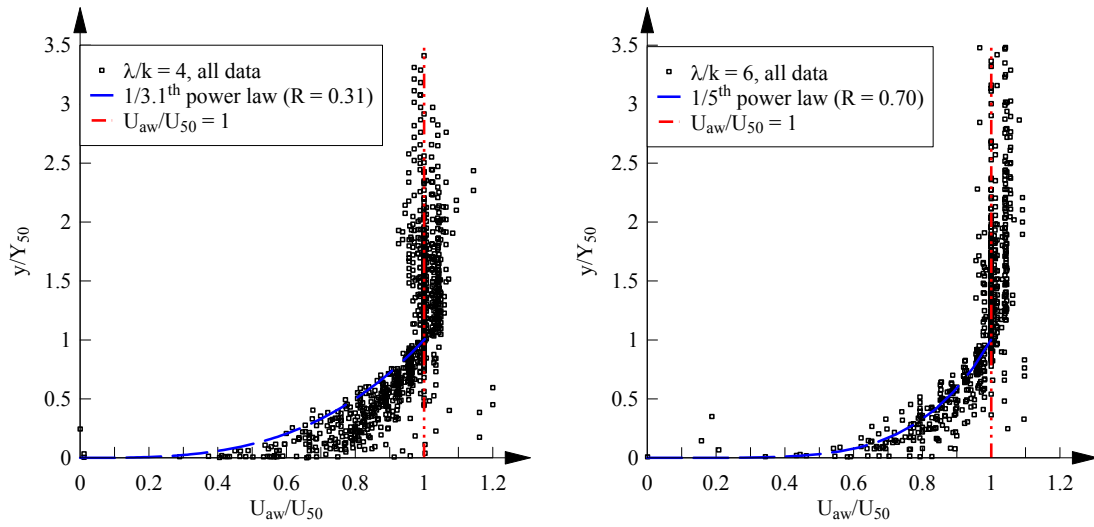


(a) model *I*



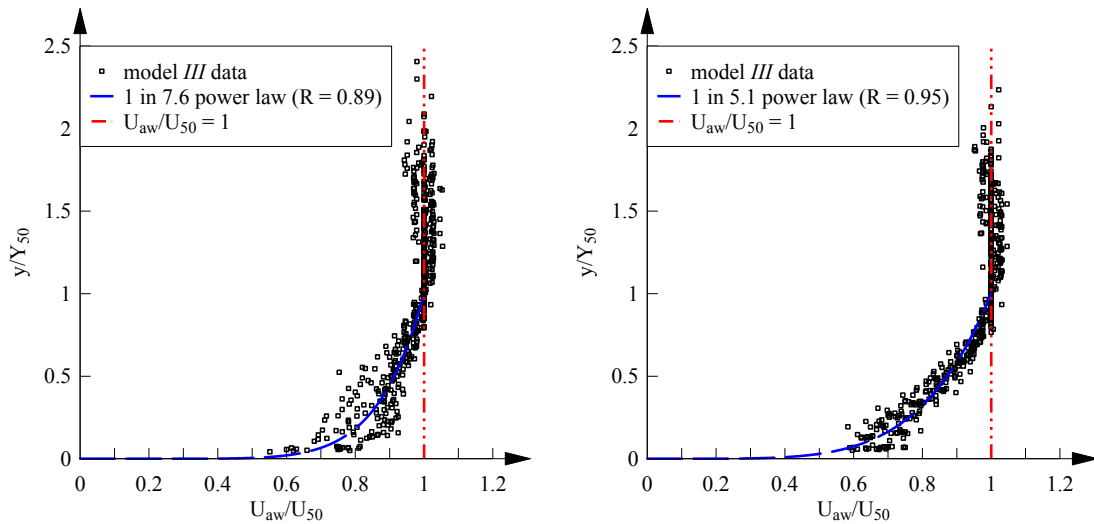
(b) model *IIa*

Zhang, G., and Chanson, H. (2018). “Air-water flow properties in stepped chutes with modified step and cavity geometries.” *International Journal of Multiphase Flow*, Vol. 99, pp. 423-436 (DOI: 10.1016/j.ijmultiphaseflow.2017.11.009) (ISSN 0301-9322).



(c) model *IIb*

(d) model *IIc*



(e) model *III*, upstream edge

(f) model *III*, downstream edge

182 Figure 5 – Interfacial velocity distributions at step edges in chutes with various step
183 roughness types. Flow conditions: $d_c/h = 0.9 - 1.7$, $Re = 3.4 - 8.8 \times 10^5$, $\theta = 45^\circ$.

184 3.2 INTERFACIAL TURBULENCE CHARACTERISTICS

185 The fluctuations of interfacial velocity may be quantified by comparing the relative
186 widths between auto- and cross-correlation functions of the two tip signals (Chanson
187 and Toombes 2002a):

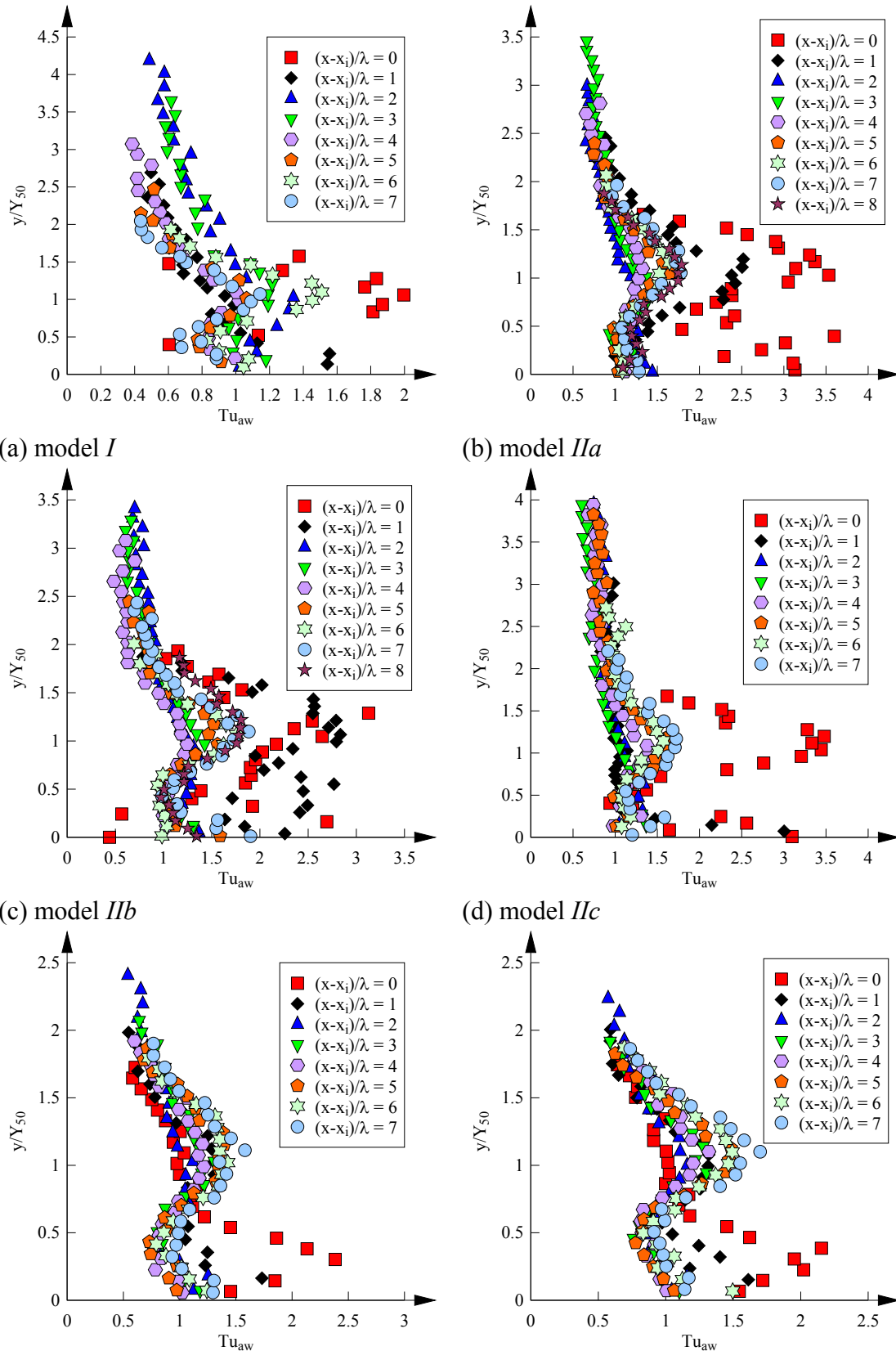
$$188 \quad Tu_{aw} = 0.85 \frac{\sqrt{\tau_{0.5}^2 - T_{0.5}^2}}{T_{aw}} = \frac{\sqrt{u_{aw}'^2}}{U_{aw}} \quad (10)$$

Zhang, G., and Chanson, H. (2018). "Air-water flow properties in stepped chutes with modified step and cavity geometries." *International Journal of Multiphase Flow*, Vol. 99, pp. 423-436 (DOI: 10.1016/j.ijmultiphaseflow.2017.11.009) (ISSN 0301-9322).

189 where Tu_{aw} is the interfacial turbulence intensity, $\tau_{0.5}$ is the time lag where the
190 normalised cross-correlation function between two probe sensors equals 0.5, $T_{0.5}$ is the
191 time lag for which the normalised auto-correlation function equals 0.5, T_{aw} is the time
192 lag corresponding to the peak of the cross-correlation function between two tips, and
193 u'_{aw} is the interfacial velocity fluctuation. For a given probe tip separation, a large
194 relative width between auto- and cross-correlation functions must correspond to large
195 fluctuations of the air-water interfaces (Chanson and Carosi 2007). Implicitly, Tu_{aw}
196 takes into account all forms of interfacial fluctuations whether they are turbulence-
197 induced rigid-body transformations (which preserve angles and line lengths) or
198 deformation of the interfaces (warping).

199 Figure 6 shows typical interfacial turbulence intensity distributions at step edges for a
200 skimming flow $d_c/h = 0.9$. For all models, the inception point data showed some large
201 scatter that reflected the unsteady nature of the region. Further downstream, the data
202 generally followed a characteristic shape, with local maxima next to the pseudo-bottom
203 and at about $y/Y_{50} = 1$. The observations were consistent with past studies in skimming
204 flows (e.g. Chanson and Carosi 2007, Felder and Chanson 2009). The two peaks in Tu_{aw}
205 were respectively associated with large turbulence levels in the step-induced wakes, and
206 a continuous breakdown of freshly entrained air coupled with a phase change process.
207 For $y/Y_{50} > 1$ the data decreased monotonically with increasing elevation. At sufficiently
208 high elevations the flow was mainly composed of discrete droplets, and the strain field
209 of the surrounding air had little effect on the water because of the large density
210 difference. The non-trivial Tu_{aw} values (> 0.5) in this region most likely resulted from
211 inhomogeneous droplet shapes instead of turbulence. A comparison between the
212 different models revealed the largest Tu_{aw} for the modified cavities, followed by those
213 for the chamfered steps and for the unmodified chute. The observation suggested that
214 interfacial turbulence might be sensitive to additional length scales introduced by
215 modifications of step and cavity shapes.

216



217 Figure 6 – Interfacial turbulence intensity distributions at step edges in chutes with
 218 various step roughness types. Flow conditions: $d_c/h = 0.9$, $Re = 3.4 \times 10^5$, $\theta = 45^\circ$.

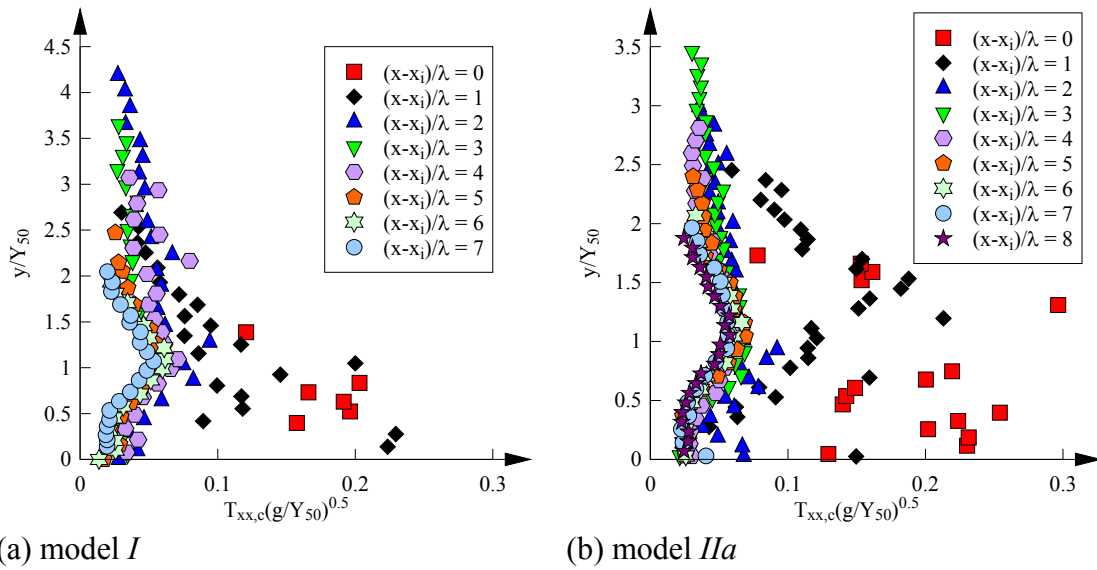
Zhang, G., and Chanson, H. (2018). “Air-water flow properties in stepped chutes with modified step and cavity geometries.” *International Journal of Multiphase Flow*, Vol. 99, pp. 423-436 (DOI: 10.1016/j.ijmultiphaseflow.2017.11.009) (ISSN 0301-9322).

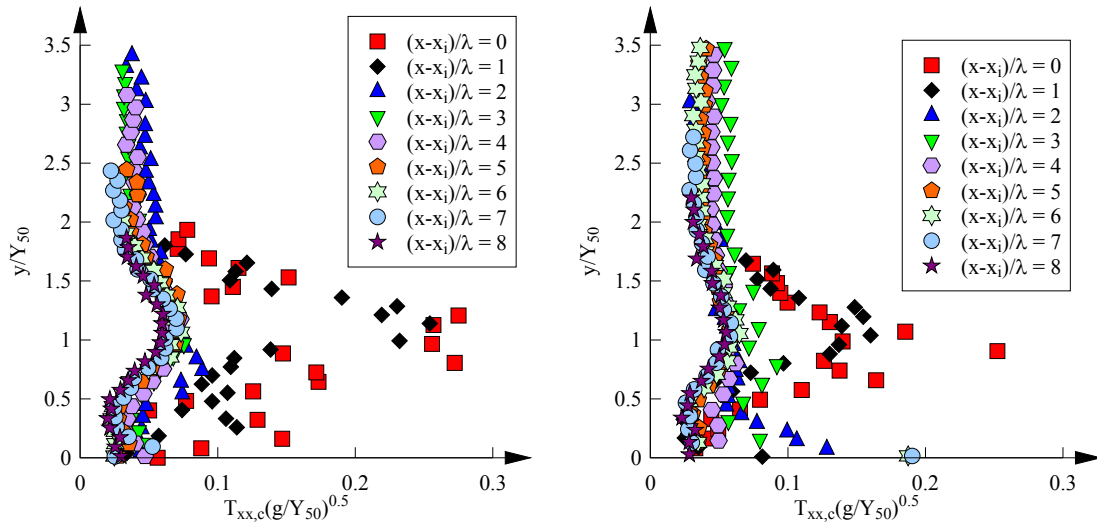
219 Following Chanson and Carosi (2007), an integral air-water time scale may be
 220 determined from the autocorrelation function of an air-water voltage signal:

$$221 \quad T_{xx,c} = \int_0^{\tau_{R_{xx,c}=0}} R_{xx,c}(\tau) d\tau \quad (11)$$

222 where $R_{xx,c}$ is the normalised autocorrelation coefficient of the void fraction signal and τ
 223 is the time lag. $T_{xx,c}$ is a time scale that characterises the longest streamwise air-water
 224 connections (i.e. air-water ‘memory’ time). Figure 7 presents the $T_{xx,c}$ distributions at
 225 step edges for a skimming flow discharge $d_c/h = 0.9$. All data followed a bell shape with
 226 a maximum at $y/Y_{50} \approx 1$. In addition, a local maximum was sometimes observed next to
 227 the pseudo-bottom, which could be linked to vortices shed from the step edge. Some
 228 large data scatter was seen for the first 2 – 3 step edges downstream of the inception
 229 point because of boundary layer fluctuations. Further downstream, the data tended to
 230 become approximately self-similar, as previously observed (Carosi and Chanson 2006,
 231 Felder 2013). The finding suggested that the air-diffusion layer could attain some local
 232 equilibrium at sufficient distance downstream of the inception point. The step edge and
 233 cavity modifications appeared to bear no significant effect on the air-water time scale
 234 distributions.

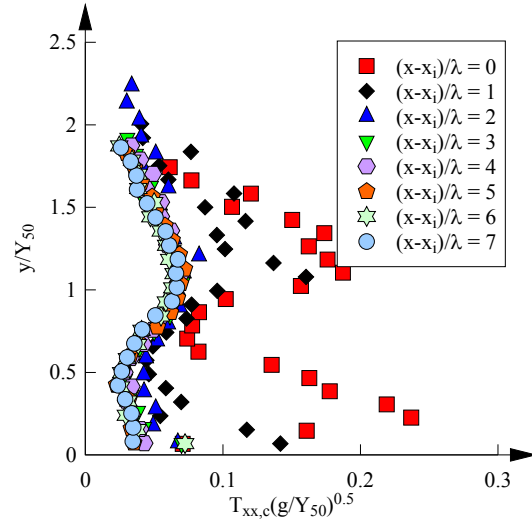
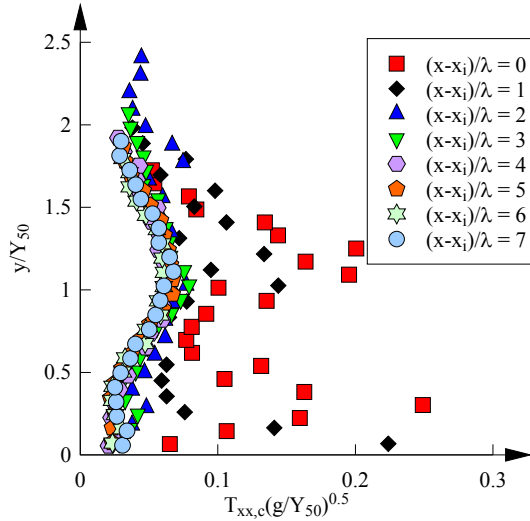
235





(c) model *IIB*

(d) model *IIC*



(e) model *III*, upstream edge

(f) model *III*, downstream edge

236 Figure 7 – Integral air-water time scale distributions at step edges in chutes with various
 237 step roughness types. Flow conditions: $d_c/h = 0.9$, $Re = 3.4 \times 10^5$, $\theta = 45^\circ$.

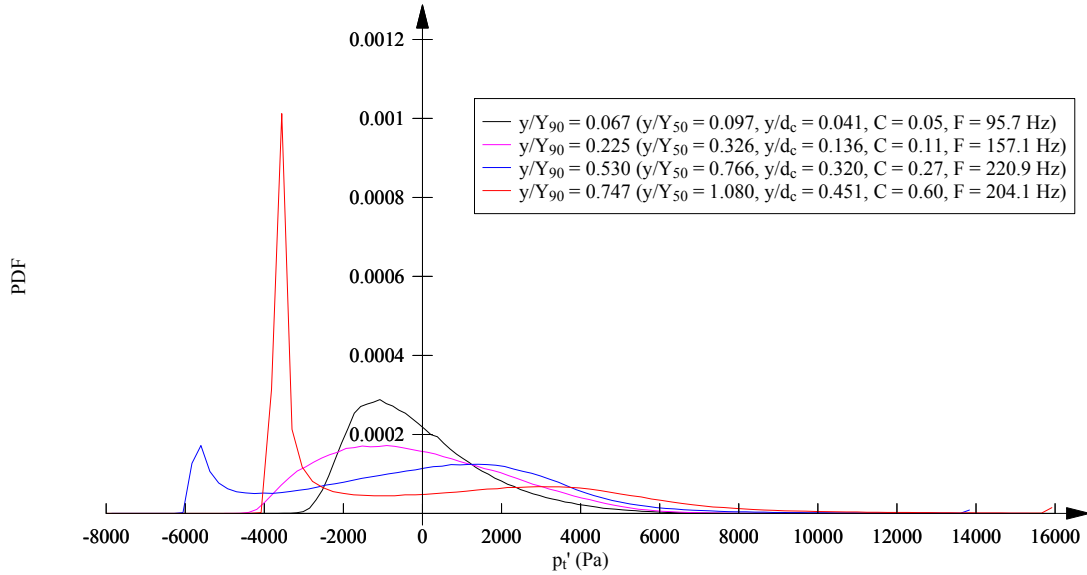
238 4. TWO-PHASE INTERACTIONS

239 4.1 TOTAL PRESSURE FLUCTUATIONS

240 The total pressure fluctuations in the aerated flow region were examined for all models
 241 with a total pressure transducer. The sensor responded to both turbulence-induced and
 242 density-induced fluctuations, as shown in Figure 8. Next to the pseudo-bottom, the PDF
 243 of the fluctuating total pressure p'_t was typically unimodal with a positive skew, likely
 244 associated with intermittent fluid ejections from the step cavity. With increasing
 245 distance from the pseudo-bottom the PDF curves became distinctively bimodal because
 246 of density fluctuations, while some bias due to wetting and drying were also likely.

Zhang, G., and Chanson, H. (2018). “Air-water flow properties in stepped chutes with modified step and cavity geometries.” *International Journal of Multiphase Flow*, Vol. 99, pp. 423-436 (DOI: 10.1016/j.ijmultiphaseflow.2017.11.009) (ISSN 0301-9322).

247 Importantly, Figure 8 implies that any second or higher order statistics of total pressure
 248 fluctuations would be determined by the combined effects of density and isolated-phase
 249 (air or water) fluctuations.



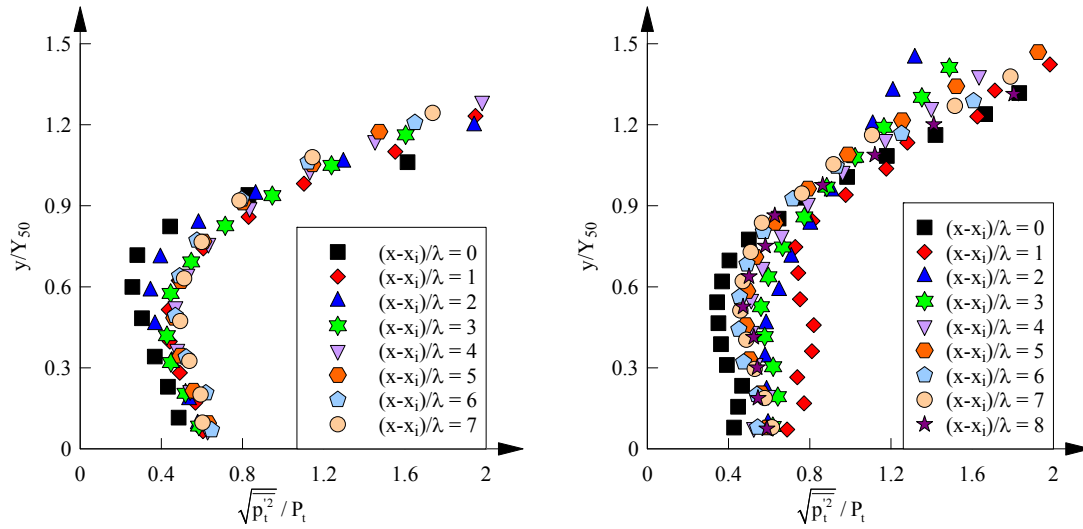
250

251 Figure 8 – Typical PDFs of total pressure fluctuations in the air-water flow region in
 252 skimming flows – Flow conditions: $d_c/h = 0.9$, $\theta = 45^\circ$, model *I*, step edge 12.

253 An intensity of total pressure fluctuation may be defined as:

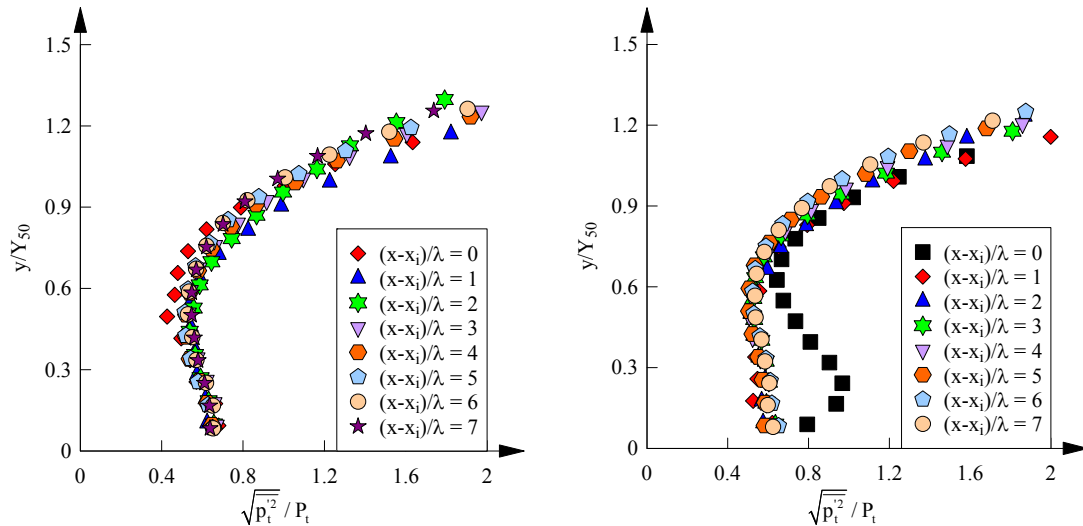
$$254 \quad \frac{\sqrt{\overline{p_t'^2}}}{P_t} \quad (12)$$

255 where p_t' and P_t are respectively the fluctuating and mean total pressure measured by the
 256 total pressure sensor. Figure 9 presents typical distributions of total pressure fluctuation
 257 intensity at step edges for a skimming flow $d_c/h = 0.9$. For all models, the total pressure
 258 fluctuation intensity exhibited a minimum at about $y/Y_{50} = 0.6$, where the void fraction C
 259 was about 0.2 – 0.3. The total pressure fluctuations intensified next to the pseudo-bottom
 260 and towards the free-surface, respectively on account of a high turbulence level and
 261 density fluctuations coupled with a diminishing mean total pressure P_t . Note that the
 262 influence due to capillary effects might grow near the free-surface. Overall, the data
 263 highlighted the turbulent nature of the skimming stepped chute flow. No significant
 264 difference was observed between the unmodified model and those with altered step and
 265 cavity geometries.



(a) model *I*, $d_c/h = 0.9$

(b) model *IIIa*



(c) model *III*, upstream edge

(d) model *III*, downstream edge

266 Figure 9 – Total pressure fluctuation intensity distributions at step edges. Flow
 267 conditions: model *I/III*: $d_c/h = 0.9$, $Re = 3.4 \times 10^5$; model *IIIa*: $d_c/h = 0.94$, $Re = 3.6 \times$
 268 10^5 ; $\theta = 45^\circ$.

269 4.2 WATER-PHASE TURBULENCE

270 The stepped spillway flow is characterised by extremely complex interactions between
 271 the air and water phases. The lowest order descriptor of the water phase turbulence is
 272 the turbulence intensity, defined as:

273
$$Tu_p = \frac{\sqrt{u_w'^2}}{U_w} \quad (13)$$

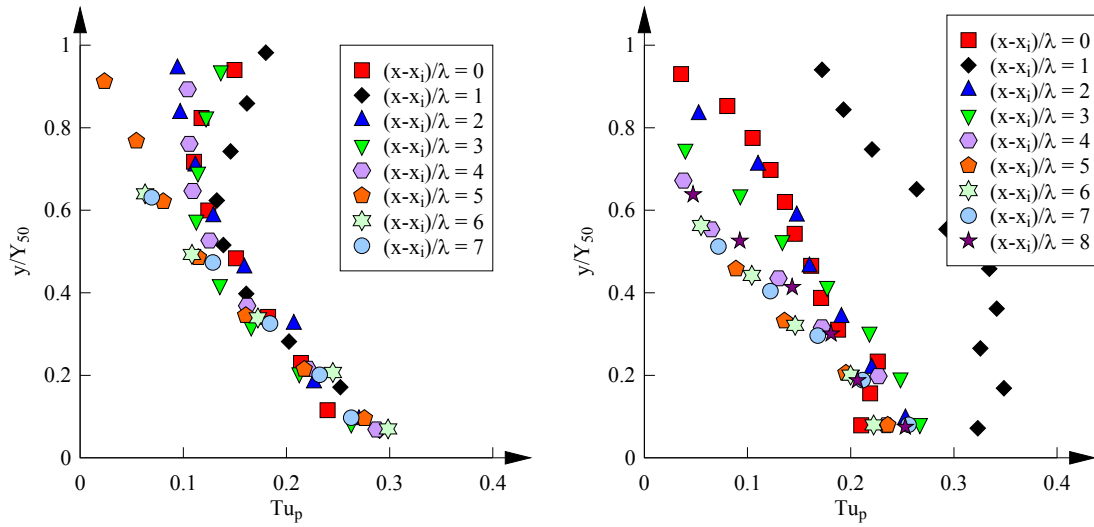
Zhang, G., and Chanson, H. (2018). "Air-water flow properties in stepped chutes with modified step and cavity geometries." *International Journal of Multiphase Flow*, Vol. 99, pp. 423-436 (DOI: 10.1016/j.ijmultiphaseflow.2017.11.009) (ISSN 0301-9322).

274 where u'_w and U_w are the fluctuating and mean water velocities. The turbulence intensity
 275 Tu_p may be estimated from simultaneously sampled total pressure and phase-detection
 276 probe signals (Zhang and Chanson 2016b):

$$277 \quad Tu_p = \sqrt{\frac{\frac{\overline{p_t^2}}{\rho_w^2 U_w^4} - \frac{1}{4} C(1-C)}{\left(1 + \frac{1}{2} C\right)(1-C)}} \quad (14)$$

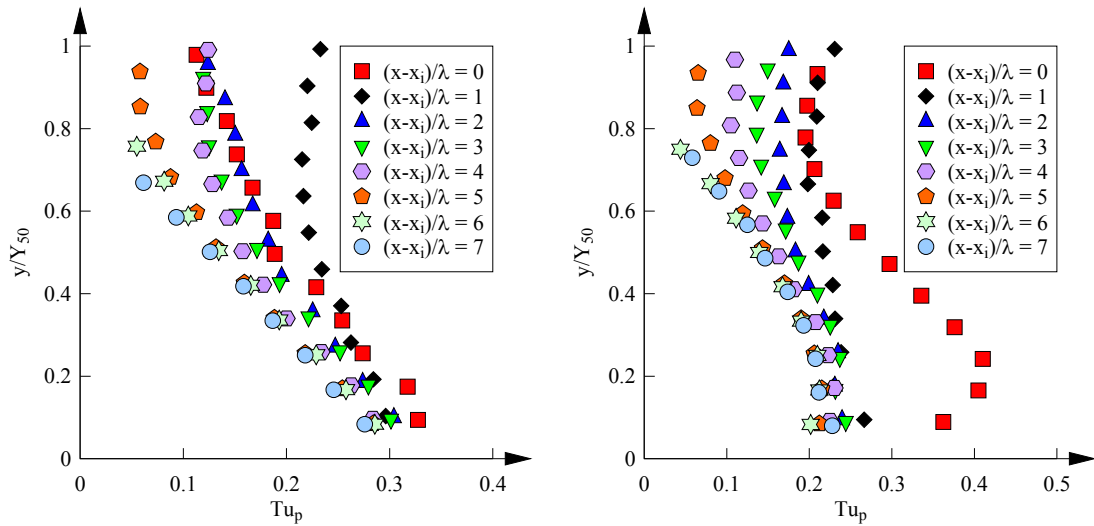
278 where the total pressure fluctuation p'_t and the void fraction C are measured by the
 279 pressure transducer and phase-detection probe, respectively. Note that the validity of
 280 Equation (14) decreases for Tu_p greater than 0.4 – 0.5. Tu_p characterises the streamwise
 281 velocity fluctuations of water particles and may be biased by: (a) instantaneous pressure
 282 rise due to surface tension during interfacial processes; (b) wetting and drying time of
 283 the sensor diaphragm; (c) bursting bubbles. Lastly, in high void fraction regions the
 284 water-phase is no longer continuous, and Equation (14) essentially reflects the velocity
 285 variations over a streamwise ensemble of water droplets.

286 Typical water phase turbulence intensity distributions at step edges are presented in
 287 Figure 10 for a skimming flow $d_c/h = 0.9$. The data were shown up to $y = Y_{50}$ because of
 288 different flow structures in the upper region. Herein the mean water velocity U_w was
 289 calculated from the mean total pressure P_t assuming a hydrostatic pressure distribution
 290 between $0 \leq y \leq Y_{90}$. All data typically ranged between 0.1 – 0.5, approximately an
 291 order of magnitude smaller than the largest interfacial turbulence intensity Tu_{aw} . Hence
 292 bubbles should not be used as accurate tracers of water-phase turbulence. Albeit some
 293 scatter, the Tu_p levels was about 30% at the pseudo-bottom, and decreased to 10% –
 294 20% at $y/Y_{50} = 0.7 – 0.8$. These values were comparable to those obtained in the clear-
 295 water flow region in a stepped chute (Ohtsu and Yasuda 1997, Amador et al. 2006), and
 296 in flows over transverse rib-roughness (Okamoto et al. 1993, Cui et al. 2003). At higher
 297 elevations, the water-phase turbulence intensities were noticeably larger next to the
 298 inception point than further downstream, highlighting the turbulent nature of the RVF
 299 region. For the chamfered steps, slightly larger Tu_p values were identified at the
 300 upstream edge than at the downstream edge. Overall, no significant cavity and step edge
 301 effects were observed on the distributions of water-phase turbulence.



(a) model I, $d_c/h = 0.9$

(b) model IIIa



(c) model III, upstream edge

(d) model III, downstream edge

302 Figure 10 – Water-phase turbulence intensity distributions at step edges in chutes with
 303 various step roughness types. Flow conditions: model III: $d_c/h = 0.9$, $Re = 3.4 \times 10^5$;
 304 model IIb: $d_c/h = 0.94$, $Re = 3.6 \times 10^5$; $\theta = 45^\circ$.

305 4.3 TOTAL PRESSURE TIME SCALES

306 The longest connections of total pressure fluctuations in the flow may be characterised
 307 by the total pressure autocorrelation time scale:

$$308 \quad T_{xx,p} = \int_0^{\tau_{R_{xx,p}=0}} R_{xx,p}(\tau) d\tau \quad (15)$$

Zhang, G., and Chanson, H. (2018). “Air-water flow properties in stepped chutes with modified step and cavity geometries.” *International Journal of Multiphase Flow*, Vol. 99, pp. 423-436 (DOI: 10.1016/j.ijmultiphaseflow.2017.11.009) (ISSN 0301-9322).

309 where $R_{xx,p}$ is the normalised autocorrelation coefficient of the total pressure signal and τ
 310 is the time lag. $T_{xx,p}$ is a measure of the average longitudinal size of the energy-
 311 containing eddies subject to effects of coherent density fluctuations.

312 Figure 11 shows typical distributions of dimensionless total pressure time scales at step
 313 edges for the various configurations. All configurations, except for model *Ila*, exhibited
 314 the largest total pressure time scales close to the pseudo-bottom, reaching a
 315 dimensionless value of approximately 0.2. The more scattered $T_{xx,p}$ data in model *Ila*
 316 appeared to be associated with increased flow instabilities caused by the cavity
 317 blockage. Significant time scales were sometimes observed next to the inception point,
 318 highlighting the large-scale instabilities in that region. For model *III*, subtly larger $T_{xx,p}$
 319 values were identified at the upstream edge than at the downstream edge. The
 320 observation could be linked to a reduction in turbulent production along the chamfer
 321 edge because of smaller velocity gradients. At sufficient distance downstream of the
 322 inception point (i.e. $(x-x_i)/\lambda > 2$), the data in both models *I* and *III* exhibited some self-
 323 similarity. Hence the energy-containing structures might have reached a state of pseudo-
 324 dynamic equilibrium, despite that uniform equilibrium flow conditions were not
 325 achieved. Importantly, the findings demonstrated some large impact of cavity blockage
 326 on the spatial homogeneity of the flow.

327 The dimensionless $T_{xx,p}$ profile displayed a marked change at about $y/Y_{50} = 0.8 - 1$. This
 328 implied a physical demarcation in flow properties about this region, potentially
 329 underpinned by structural changes in the two-phase turbulence patterns. In the lower
 330 region (i.e. $y/Y_{50} < 0.8 - 1$), the $T_{xx,p}$ values were dominantly of the order 0.1, which was
 331 comparable to a roughness timescale T_k defined as:

$$332 \quad T_k = \frac{k}{U_{sl}} \quad \text{for } 0 \leq y/Y_{50} < 0.8 - 1 \quad (16)$$

333 where k is the roughness height projection normal to the pseudo-bottom, and U_{sl} is the
 334 convection velocity in the shear layer. Since $T_{xx,p} \sim k_T/\varepsilon$ (k_T : turbulent kinetic energy; ε :
 335 dissipation) (Pope 2000), the observation highlighted the importance of the lower
 336 aerated flow region for turbulent production, and the absence of roughness
 337 characteristics for $y/Y_{50} > 0.8 - 1$.

Zhang, G., and Chanson, H. (2018). "Air-water flow properties in stepped chutes with modified step and cavity geometries." *International Journal of Multiphase Flow*, Vol. 99, pp. 423-436 (DOI: 10.1016/j.ijmultiphaseflow.2017.11.009) (ISSN 0301-9322).

338 Figure 12 examines the relationship between the dimensionless total pressure time scale
 339 $T_{xx,p}$ and integral air-water time scale $T_{xx,c}$ in stepped chutes *I* and *IIa*. The data revealed
 340 a strong correlation between the two variables for $y/Y_{50} \geq 1$ ($R = 0.79$), and almost no
 341 correlation for $y/Y_{50} < 1$ ($R = 0.13$), where R is the normalised correlation coefficient. If
 342 the total pressure signal is simply expressed as a sum of air and water components:

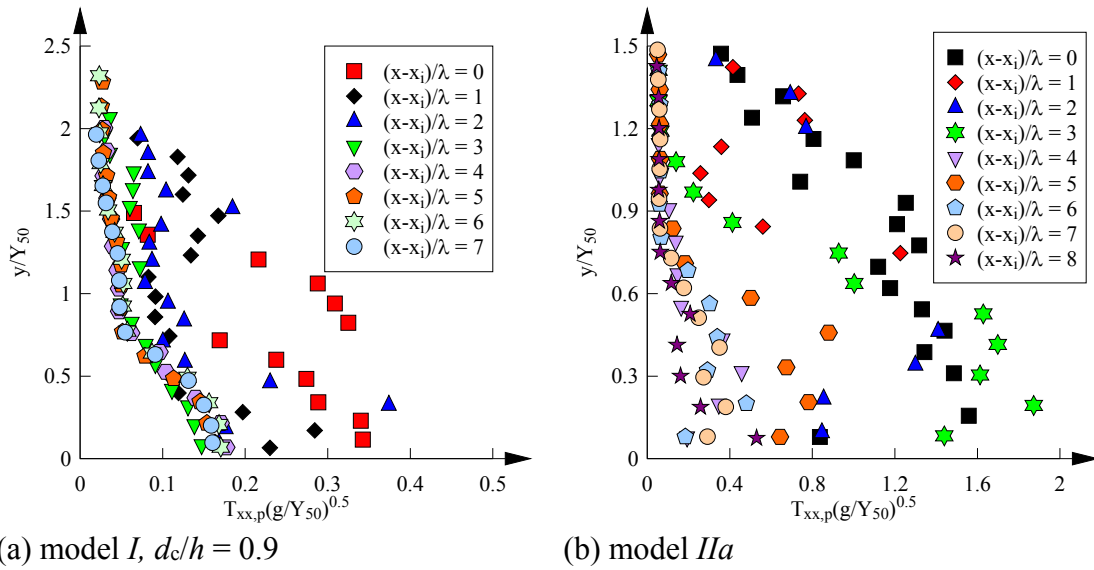
$$343 \quad f(t) = f_a(t) + f_w(t) \quad (17)$$

344 and assuming that the air and water components are independent, it follows that:

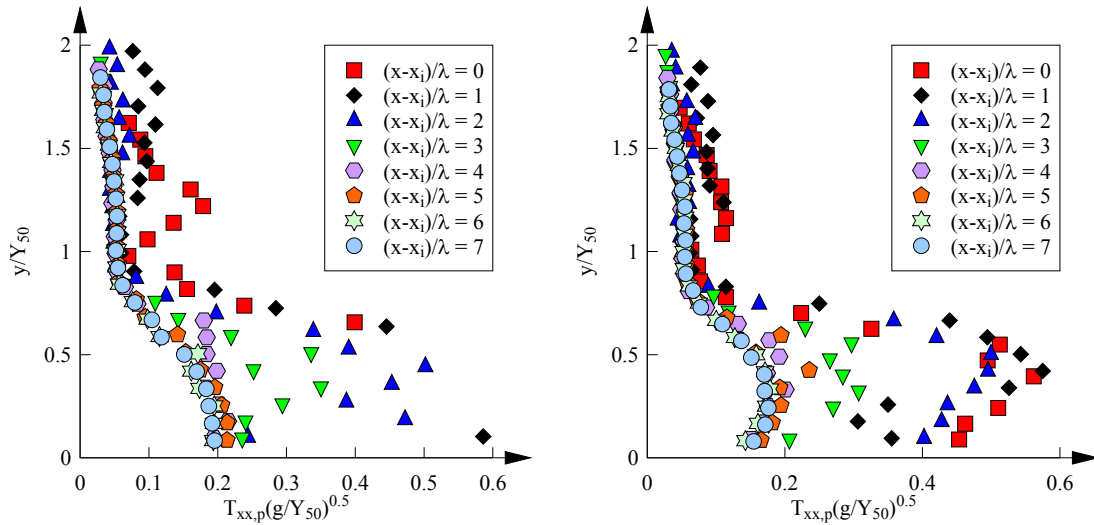
$$345 \quad R_{xx,p}(\tau) = R_{xx,a}(\tau) + R_{xx,w}(\tau) \quad (18)$$

$$346 \quad T_{xx,p} = T_{xx,c} + T_{xx,w} \quad (19)$$

347 where $R_{xx,w}$ and $T_{xx,w}$ are the water-phase contributions to the autocorrelation function
 348 and integral time scale of the total pressure signal. For $y/Y_{50} \geq 1$, the high correlation
 349 between $T_{xx,p}$ and $T_{xx,c}$ implies that $T_{xx,w} \approx 0$. Hence the water-phase contribution to the
 350 total pressure signal in this region was approximately a white noise with a flat power
 351 spectrum (i.e. the autocorrelation function of the water phase signal is a delta function).
 352 The finding confirmed a lack of water-phase structure in the upper flow region. Note
 353 that the data might be skewed in very low void fraction regions due to unreliability of
 354 the phase-detection probe.



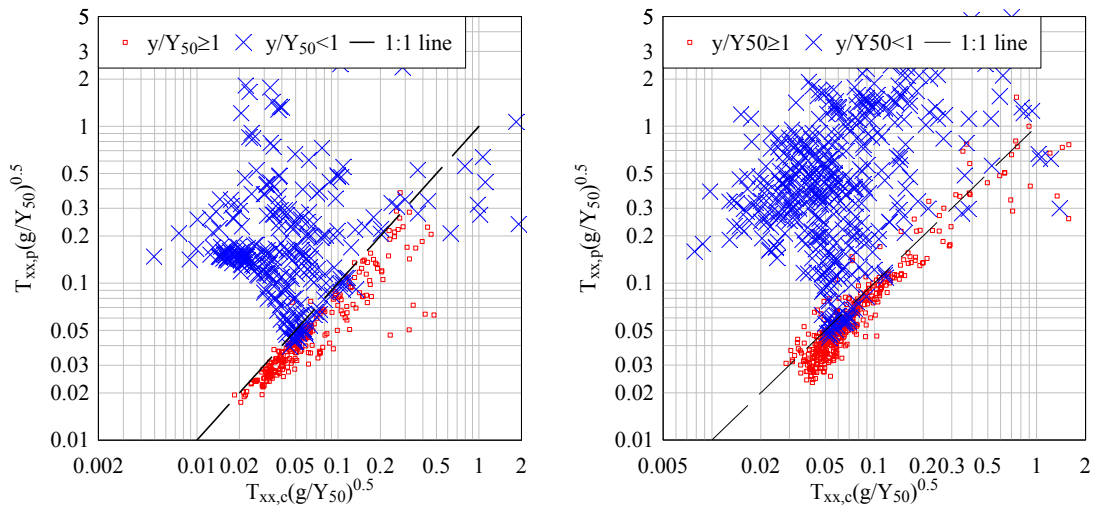
Zhang, G., and Chanson, H. (2018). “Air-water flow properties in stepped chutes with modified step and cavity geometries.” *International Journal of Multiphase Flow*, Vol. 99, pp. 423-436 (DOI: 10.1016/j.ijmultiphaseflow.2017.11.009) (ISSN 0301-9322).



(c) model III, upstream edge

(d) model III, downstream edge

355 Figure 11 – Total pressure time scale distributions at step edges in chutes with various
 356 step roughness types. Flow conditions: model I/II: $d_c/h = 0.9$, $Re = 3.4 \times 10^5$; model IIb:
 357 $d_c/h = 0.94$, $Re = 3.6 \times 10^5$; $\theta = 45^\circ$.



(a) model I

(b) model IIa

358 Figure 12 – Relationship between $T_{xx,p}$ and $T_{xx,c}$ at step edges in models I and IIa. Flow
 359 conditions: Model I: $d_c/h = 0.9 - 1.7$, $Re = 3.4 - 8.8 \times 10^5$; Model IIa: $d_c/h = 0.94 -$
 360 1.75 , $Re = 3.6 - 9.1 \times 10^5$; $\theta = 45^\circ$.

361 5. CONCLUSION

362 Skimming air-water flow properties were carefully examined in a stepped chute
 363 configured with triangular steps, chamfered steps, and partially blocked step cavities.
 364 Interactions between the air and water phases were investigated with a dual-tip phase-

Zhang, G., and Chanson, H. (2018). "Air-water flow properties in stepped chutes with modified step and cavity geometries." *International Journal of Multiphase Flow*, Vol. 99, pp. 423-436 (DOI: 10.1016/j.ijmultiphaseflow.2017.11.009) (ISSN 0301-9322).

365 detection probe mounted side-by-side with a total pressure transducer. The effects on
366 skimming flow air-water properties induced by step and cavity geometry modifications
367 were characterised.

368 Void fraction distributions in all models showed a reasonable agreement with analytical
369 solutions of the advection-diffusion equation. The no-flux boundary condition imposed
370 on the chamfer surface stipulated an air boundary layer growth, which could lead to a
371 reduction in skin friction. All bubble count rate data followed a characteristic shape with
372 a maximum occurring next to $C \approx 0.5$. The interfacial velocity data followed a two-tier
373 distribution with a demarcation at $y/Y_{50} \approx 1$. In comparison to the un-modified step
374 geometry, steeper and flatter step edge velocity profiles were respectively observed for
375 the chamfered steps and partially blocked cavities. Correlation analyses identified
376 significant interfacial fluctuations and large air-water structures at $y/Y_{50} \approx 1$ as well as
377 next to the pseudo-bottom, which might be sensitive to step and cavity geometry
378 modifications. The data indicated that uniform equilibrium conditions were not
379 achieved in the present studies.

380 Simultaneously acquired void fraction and total pressure signals permitted individual
381 examinations of the component phases. Significant total pressure fluctuations were
382 identified throughout the flow column, resulting from water-phase turbulent fluctuations
383 coupled with rapid phase changes. The water-phase turbulence levels were comparable
384 to those reported for the clear water flow region, and were substantially less than the
385 interfacial turbulence levels. The total pressure time scale distributions implied a
386 physical demarcation about $y/Y_{50} = 0.8 - 1$, where the upper region was characterised by
387 a lack of coherent water-phase structures. The partial cavity blockage also appeared to
388 result in increased instabilities in the aerated flow region.

389 The present investigation indicated some implications for stepped chute design due to
390 step edge and cavity modifications. The chamfers led to some reduction in air
391 entrainment, slightly raised interfacial turbulence levels, and a steeper mean velocity
392 profile next to the pseudo-bottom. The partial cavity blockages were observed to cause
393 flow instabilities and an increased presence of large-scale structures in the overflow,
394 likely resulting from modifications to the vortex shedding dynamics. Importantly, the

Zhang, G., and Chanson, H. (2018). "Air-water flow properties in stepped chutes with modified step and cavity geometries." *International Journal of Multiphase Flow*, Vol. 99, pp. 423-436 (DOI: 10.1016/j.ijmultiphaseflow.2017.11.009) (ISSN 0301-9322).

395 results highlighted the turbulent nature and extremely complex air-water interactions in
396 aerated skimming flows over stepped roughness.

397 **6. ACKNOWLEDGEMENTS**

398 The authors thank Jason Van Der Gevel and Steward Matthews (University of
399 Queensland, Australia) for their technical assistance. The financial support of Australian
400 Research Council (Grant DP120100481) is acknowledged. The first author was a
401 recipient of Australian Postgraduate Award.

402 **7. REFERENCES**

403 Amador, A., Sánchez-Juny, M. and Dolz, J. (2006). "Characterization of the nonaerated
404 flow region in a stepped spillway by PIV." *Journal of Fluids Engineering*, ASME,
405 Vol. 128, No. 6, pp. 1266-1273 (DOI: 10.1115/1.2354529).

406 Carosi, G., and Chanson, H. (2006). "Air-water time and length scales in skimming
407 flow on a stepped spillway. Application to the spray characterisation." *Report No.*
408 *CH59/06*, Division of Civil Engineering, The University of Queensland, Brisbane,
409 Australia, July, 142 pages.

410 Chanson, H. (1993). "Stepped spillway flows and air entrainment." *Canadian Journal*
411 *of Civil Engineering*, Vol. 20, No. 3, June, pp. 422-435 (DOI: 10.1139/193-057).

412 Chanson, H. (1995). "Air bubble diffusion in supercritical open channel flow." *Proc.*
413 *12th Australasian Fluid Mechanics Conference*, Sydney, Australia, R.W.
414 BILGER Ed., Vol. 2, pp. 707-710.

415 Chanson, H. (1997). "Air bubble entrainment in open channels. Flow structure and
416 bubble size distributions." *International Journal of Multiphase Flow*, Vol. 23, No.
417 1, pp. 193-203 (DOI: 10.1016/S0301-9322(96)00063-8).

418 Chanson, H. (2001a). "The hydraulics of stepped chutes and spillways." Balkema,
419 Lisse, The Netherlands, 418 pages.

420 Chanson, H. (2001b). "Hydraulic design of stepped spillways and downstream energy
421 dissipators." *Dam Engineering*, Vol. 11, No. 4, pp. 205-242.

- Zhang, G., and Chanson, H. (2018). "Air-water flow properties in stepped chutes with modified step and cavity geometries." *International Journal of Multiphase Flow*, Vol. 99, pp. 423-436 (DOI: 10.1016/j.ijmultiphaseflow.2017.11.009) (ISSN 0301-9322).
- 422 Chanson, H. (2002). "Air-water flow measurements with intrusive phase-detection
423 probes. Can we improve their interpretation?" *Journal of Hydraulic Engineering*,
424 ASCE, Vol. 128, No. 3, pp. 252-255 (DOI: 10.1061/(ASCE)0733-
425 9429(2002)128:3(252)).
- 426 Chanson, H. (2004). "Drag reduction in skimming flow on stepped spillways by
427 aeration." *Journal of Hydraulic Research*, IAHR, Vol. 42, No. 3 , pp. 316-322.
- 428 Chanson, H., and Carosi, G. (2007). "Advanced post-processing and correlation
429 analyses in high-velocity air-water flows" *Environmental Fluid Mechanics*, Vol.
430 7, No. 6, pp. 495-508.
- 431 Chanson, H., and Toombes, L. (2002a). "Air-Water Flows down Stepped chutes:
432 Turbulence and Flow Structure Observations." *International Journal of*
433 *Multiphase Flow*, Vol. 28, No. 11, pp. 1737-1761 (DOI: 10.1016/s0301-
434 9322(02)00089-7).
- 435 Chanson, H., and Toombes, L. (2002b). "Energy dissipation and air entrainment in
436 stepped storm waterway. experimental study." *Journal of Irrigation and Drainage*
437 *Engineering*, ASCE, Vol. 128, No. 5, pp. 305-315 (DOI: 10.1061/(asce)0733-
438 9437(2002)128:5(305)).
- 439 Chanson, H., Yasuda, Y., and Ohtsu, I. (2002). "Flow resistance in skimming flows and
440 its modelling." *Canadian Journal of Civil Engineering*, Vol. 29, No. 6, pp. 809-
441 819 (DOI: 10.1139/l02-083).
- 442 Crowe, C., Sommerfeld, M., and Tsuji, Y (1998). "Multiphase flows with droplets and
443 particles." CRC Press, Boca Raton, USA, 471 pages (ISBN 0-8493-9469-4).
- 444 Cui, J., Patel, V.C. and Lin, C. (2003). "Large-eddy simulation of turbulent flow in a
445 channel with rib roughness." *International Journal of Heat and Fluid Flow*, Vol.
446 24, No. 3, pp. 372-388 (DOI: 10.1016/s0142-727x(03)00002-x).
- 447 Felder, S., and Chanson, H. (2009). "Turbulence, dynamic similarity and scale effects in
448 high-velocity free-surface flows above a stepped chute." *Experiments in Fluids*,
449 Vol. 47, No. 1, pp. 1-18 (DOI: 10.1007/s00348-009-0628-3).

- Zhang, G., and Chanson, H. (2018). "Air-water flow properties in stepped chutes with modified step and cavity geometries." *International Journal of Multiphase Flow*, Vol. 99, pp. 423-436 (DOI: 10.1016/j.ijmultiphaseflow.2017.11.009) (ISSN 0301-9322).
- 450 Felder, S. (2013). "Air-water flow properties on stepped spillways for embankment
451 dams. Aeration, energy dissipation and turbulence on uniform, non-uniform and
452 pooled stepped chutes." *Ph.D. Thesis*, School of Civil Engineering, The
453 University of Queensland, Brisbane, Australia.
- 454 Felder, S., and Chanson, H. (2014a). "Triple decomposition technique in air–water
455 flows: application to instationary flows on a stepped spillway." *International
456 Journal of Multiphase Flow*, Vol. 58, pp. 139-153 & 3 videos (DOI:
457 10.1016/j.ijmultiphaseflow.2013.09.006).
- 458 Felder, S., and Chanson, H. (2014b). "Effects of step pool porosity upon flow aeration
459 and energy dissipation on pooled stepped spillways." *Journal of Hydraulic
460 Engineering*, ASCE, Vol. 140, No. 4, Paper 04014002, 11 pages (DOI:
461 10.1061/(ASCE)HY.1943-7900.0000858).
- 462 Felder, S., and Chanson, H. (2016). "Air–water flow characteristics in high-velocity
463 free-surface flows with 50% void fraction." *International Journal of Multiphase
464 Flow*, Vol. 85, pp. 186-195 (DOI: 10.1016/j.ijmultiphaseflow.2016.06.004).
- 465 Gonzalez, C.A., and Chanson, H. (2008). "Turbulence manipulation in embankment
466 stepped chute flows: an experimental study." *European Journal of Mechanics
467 B/Fluids*, Vol. 27, No. 4, pp. 388-408 (DOI: 10.1016/j.euromechflu.2007.09.003).
- 468 Ohtsu, I. and Yasuda, Y. (1997). "Characteristics of flow conditions on stepped
469 channels". *Proc. 27th IAHR Congress*, Theme D, San Francisco, USA, pp. 583-
470 588.
- 471 Okamoto, S., Seo, S., Nakaso, K. and Kawai, I. (1993). "Turbulent shear flow and heat
472 transfer over the repeated two-dimensional square ribs on ground plane." *Journal
473 of Fluids Engineering*, ASME, Vol. 115, No. 4, pp. 631-637 (DOI:
474 10.1115/1.2910191).
- 475 Pope, S. (2000). "Turbulent flows", Cambridge University Press, Cambridge, U.K.
- 476 Rao, N.S.L. and Kobus, H.E. (1971). "Characteristics of self-aerated free-surface
477 flows." *Water and Waste Water Current Research and Practice*. Vol.10, Eric
478 Schmidt Verlag, Berlin.

- Zhang, G., and Chanson, H. (2018). "Air-water flow properties in stepped chutes with modified step and cavity geometries." *International Journal of Multiphase Flow*, Vol. 99, pp. 423-436 (DOI: 10.1016/j.ijmultiphaseflow.2017.11.009) (ISSN 0301-9322).
- 479 Stephenson, D. (1988). "Stepped Energy Dissipators." *Proc. Intl Symp. on Hydraulics*
480 *for High Dams*, IAHR, Beijing, China, pp. 1228-12-35.
- 481 Toombes, L., and Chanson, H. (2008). "Interfacial aeration and bubble count rate
482 distributions in a supercritical flow past a backward-facing step." *International*
483 *Journal of Multiphase Flow*, Vol. 34, No. 5, pp. 427-436.
- 484 Wood, I.R. (1985). "Air water flows" *Proc. 21st IAHR Congress*, Melbourne, Australia,
485 pp. 18-29.
- 486 Wood, I.R. (1991). "Air entrainment in free-surface flows." *IAHR Hydraulic Structures*
487 *Design Manual No. 4*, Balkema Publ., Rotterdam.
- 488 Zhang, G., and Chanson, H. (2016a). "Gabion stepped spillway: interactions between
489 free-surface, cavity, and seepage flows." *Journal of Hydraulic Engineering*,
490 ASCE, Vol. 142, No. 5, Paper 06016002, 5 pages (DOI:
491 10.1061/(ASCE)HY.1943-7900.0001120).
- 492 Zhang, G., and Chanson, H. (2016b). "Interactions between free-surface aeration and
493 total pressure on a stepped chute." *Experimental Thermal and Fluid Science*, Vol.
494 74, pp. 368-381 (DOI: 10.1016/j.expthermflusci.2015.12.011).
- 495 Zhang, G., and Chanson, H. (2017). "Self-aeration in smooth and stepped chutes."
496 *Environmental Fluid Mechanics*, Vol. 17, No. 1, pp. 27-46 (DOI:
497 10.1007/s10652-015-9442-z).

498 **APPENDIX A. LIST OF SYMBOLS**

- 499 C time-averaged void fraction (-);
- 500 C_{mean} depth-averaged void fraction (-);
- 501 D_a average diffusivity (m^2/s);
- 502 D_t turbulent diffusivity (m^2/s);
- 503 D_0 dimensionless diffusivity (-);
- 504 d_c critical depth (m);
- 505 F bubble count rate (Hz);

Zhang, G., and Chanson, H. (2018). "Air-water flow properties in stepped chutes with modified step and cavity geometries." *International Journal of Multiphase Flow*, Vol. 99, pp. 423-436 (DOI: 10.1016/j.ijmultiphaseflow.2017.11.009) (ISSN 0301-9322).

506	g	gravity constant (m/s^2);
507	h	vertical step height (m);
508	K	integration constant (-);
509	k	step roughness height (m);
510	k_T	turbulent kinetic energy (m^2/s^2);
511	l	horizontal step length (m);
512	N_{50}	power law exponent (-);
513	P_t	time-averaged total pressure (Pa);
514	p_t'	fluctuating total pressure (Pa);
515	Q	water discharge (m^3/s);
516	q_w	unit discharge of water (m^2/s);
517	R	normalised correlation coefficient (-);
518	$R_{xx,a}$	air-phase contribution to $R_{xx,p}$ (-);
519	$R_{xx,c}$	normalised autocorrelation coefficient of a void fraction signal (-);
520	$R_{xx,p}$	normalised autocorrelation coefficient of a total pressure signal (-);
521	$R_{xx,w}$	water-phase contribution to $R_{xx,p}$ (-);
522	Re	Reynolds number (-);
523	T_{aw}	average interfacial travel time between two probe tips (s);
524	T_k	roughness time scale (s);
525	$T_{xx,a}$	air-phase contribution to $T_{xx,p}$ (s);
526	$T_{xx,c}$	streamwise autocorrelation timescale based on a void fraction signal (s);
527	$T_{xx,p}$	streamwise autocorrelation timescale based on a total pressure signal (s);
528	$T_{xx,w}$	water-phase contribution to $T_{xx,p}$ (s);

Zhang, G., and Chanson, H. (2018). "Air-water flow properties in stepped chutes with modified step and cavity geometries." *International Journal of Multiphase Flow*, Vol. 99, pp. 423-436 (DOI: 10.1016/j.ijmultiphaseflow.2017.11.009) (ISSN 0301-9322).

529	$T_{0.5}$	time lag for which normalised autocorrelation of the leading tip equals 0.5 (s);
530	$T_{u_{aw}}$	interfacial turbulence intensity (-);
531	T_{u_p}	water-phase turbulence intensity estimated from synchronised total pressure and
532		void fraction signals (-);
533	t	time (s);
534	U_{aw}	time-averaged interfacial velocity (m/s);
535	U_{sl}	convection velocity in shear layer (m/s);
536	U_w	time-averaged water velocity (m/s);
537	U_{50}	time-averaged interfacial velocity corresponding to $C = 0.5$ (m/s);
538	u_{aw}'	fluctuating interfacial velocity (m/s);
539	x	streamwise coordinate (m);
540	Y_{50}	elevation normal to the pseudo-bottom where $C = 0.5$ (m);
541	Y_{90}	elevation normal to the pseudo-bottom where $C = 0.9$ (m);
542	y	normal coordinate (m);
543		
544	<i>Greek symbols</i>	
545	Δx	streamwise separation between probe tips (m);
546	ε	dissipation rate (m^2/s^3);
547	θ	chute slope ($^\circ$);
548	λ	streamwise separation between adjacent steps (m);
549	τ	time lag between two signals (s);
550	$\tau_{0.5}$	time lag for which the normalised cross-correlation between two probe tips
551		equals 0.5 (s);
552		

Zhang, G., and Chanson, H. (2018). "Air-water flow properties in stepped chutes with modified step and cavity geometries." *International Journal of Multiphase Flow*, Vol. 99, pp. 423-436 (DOI: 10.1016/j.ijmultiphaseflow.2017.11.009) (ISSN 0301-9322).

553 *Functions*

554 erfc complementary error function;

555

556 *Acronyms*

557 CDF cumulative distribution function;

558 DPP dual-tip phase-detection probe;

559 FS full scale;

560 GVF gradually varied flow;

561 PDF probability density function;

562 RVF rapidly varied flow;

563 TPT total pressure transducer.